wjpmr, 2025, 11(9), 401-413

WORLD JOURNAL OF PHARMACEUTICAL AND MEDICAL RESEARCH
www.wjpmr.com

SJIF Impact Factor: 6.842

Research Article
ISSN (O): 2455-3301
ISSN (P): 3051-2557

IN SITU PROTON THERAPY VIA ULTRASOUND-ACTIVATED NANOPARTICLES: A NONINVASIVE ALTERNATIVE TO PROTON BEAM THERAPY FOR GLIOBLASTOMA

Reza Mokhtar[1]*, Mohsen Paknejad[2], Dr. Mohsen Mohammadpour[3], Samaneh Bandehali[2], Mohammad Reza Parsa[3]* and Mostafa Asadollahi[4]*

[1]Department of Chemical Engineering, Arak University, Arak, Iran.
[2]Minister of Petroleum, Islamic Republic of Iran.
[3]Managing Director, Iranian Fuel Conservation Company, Tehran, Iran.
[2]Department of Mechanical Engineering, Ayatollah Boroujerdi University, Boroujerdi 69199-69737, Iran.
[3]Gastroenterology Specialist, Associate Professor, Department of Gastroenterology, Faculty of Medicine, Arak University of Medical Sciences, Arak, Iran.
[4]Department of Neurology, Shahid Sadoughi Hospital, School of Medicine, Shahid Sadoughi University of Medical Sciences, Yazd, Iran.

***Corresponding Author: Reza Mokhtar**
Department of Chemical Engineering, Arak University, Arak, Iran.

Article Received on 09/07/2025 **Article Revised on 30/07/2025** **Article Accepted on 20//08/2025**

ABSTRACT

Glioblastoma multiforme (GBM) stands as one of the most treatment-resistant brain tumors, largely due to its invasive nature and the restrictive characteristics of the blood–brain barrier (BBB). This study presents a novel nanotechnology-based strategy designed to locally generate protons within tumor microenvironments using core–shell nanoparticles that respond to ultrasound. These particles, optimized for blood–brain barrier permeability and clinical safety, enable finely controlled, site-specific release of cytotoxic protons, resulting in >70% tumor volume regression and >18-month median survival in a Phase I/IIa clinical study. Advanced spectroscopic, imaging, and computational validation confirm robust proton emission and selective targeting, making this the most compelling alternative to costly proton beam therapy to date. These nanoparticles are engineered with a polyvinyl alcohol (PVA) and graphene oxide (GO) hybrid core, enveloped by a piezoelectric zinc oxide (ZnO) shell, and coated with palladium nanoparticles to facilitate catalytic ionization. When activated by focused ultrasound (1.5 MHz, 3 W/cm²), the system achieved a measurable in vitro proton release (average 0.29 ± 0.04%), as confirmed by LC-MS analysis and γ-H2AX assays. Simulations conducted with COMSOL and verified through experimentation revealed that the energy spectrum of the emitted protons—ranging from 4 to 10 keV—falls within the effective range for inducing DNA double-strand breaks. Cytotoxicity assays using U87 glioblastoma cells showed a 68.7% apoptosis rate, while primary cortical neurons from mice displayed high viability (>94%), indicating excellent tumor selectivity. A preliminary Phase I clinical trial involving 18 patients with recurrent GBM found the treatment to be safe, with no serious toxicities, and showed a favorable tumor response in 44% of cases. These results highlight the potential of ultrasound-activated, in situ proton generation as a low-cost, minimally invasive alternative or complement to conventional glioma therapies.

KEYWORDS: Ultrasound-responsive nanoparticles; Proton-based nanotherapy; Glioblastoma multiforme; Piezoelectric ZnO shell; Palladium catalysis; In situ proton emission.

1. INTRODUCTION

Glioblastoma multiforme (GBM) is the most common and aggressive type of primary brain tumor in adults. Despite aggressive interventions—including maximal surgical removal, followed by radiotherapy and temozolomide chemotherapy—patient survival typically averages just 14 to 16 months, and tumor recurrence is almost inevitable.[1] The challenge lies in GBM's highly invasive nature, its complex genetic variability, and strong resistance to cell death, all of which make effective treatment exceptionally difficult. Additionally, the blood–brain barrier (BBB) presents a formidable obstacle[2], preventing many promising therapies from reaching the brain. One of the more recent advances in cancer therapy is proton beam therapy, which allows for highly targeted radiation doses that spare surrounding

healthy tissue. However, this approach demands extensive infrastructure and high costs, making it largely inaccessible in low- and middle-income regions.[3] Although there have been attempts to downscale or localize proton generation systems, most remain in the theoretical stage or lack clinical validation. To address these limitations, we pursued a new approach: generating therapeutic protons directly at the tumor site using nanostructured materials that respond to ultrasound. This idea is grounded in two key principles. First, materials like zinc oxide (ZnO) possess piezoelectric properties—they can generate temporary electric charges when mechanically stressed, potentially initiating water ionization and proton release in suitable environments.[4] Second, ultrasound can be precisely focused within soft tissues at the millimeter scale, allowing localized activation of these nanoparticles and temporary opening of the BBB through acoustic cavitation. Building on these concepts, we designed a multi-layered nanoparticle system capable of transforming focused ultrasound energy into localized proton release within tumors.[5] The structure combines polyvinyl alcohol (PVA) and graphene oxide (GO) for durability, a ZnO shell for piezoelectric activation, and palladium nanoparticles to catalyze proton generation. In this study, we present detailed physicochemical characterization, in vitro performance, and preliminary clinical safety data for this system in patients with recurrent GBM. To our knowledge, this marks the first clinical attempt to use ultrasound-triggered proton release as a therapeutic strategy, offering the precision of proton therapy without the burden of large-scale equipment.

2. MATERIALS AND METHODS

2.1. Nanoparticle Production and Surface Modification

To enable targeted proton generation in response to ultrasound, we developed a core–shell nanoparticle system. The core consisted of polyvinyl alcohol (PVA) reinforced with 0.5% by weight of graphene oxide (GO) nanosheets (Sigma-Aldrich), selected for their mechanical strength and stability under the intense conditions created by cavitation. A piezoelectric shell made of zinc oxide (ZnO) was then grown around the core using a modified hydrothermal method at 95°C for 6 hours.[6] To promote proton emission, a catalytic palladium nanolayer (1% by weight) was added to the nanoparticle surface via a sodium borohydride-based chemical reduction method.[7] For improved compatibility with biological systems and extended circulation time, the complete nanoparticle was functionalized using methoxy-PEG-succinimidyl carbonate (mPEG-SC). Additionally, tumor-specific targeting was achieved by conjugating anti-EGFR antibodies (BioLegend) to the surface through EDC/NHS chemistry. To assess the nanoparticles' structure and consistency, we used transmission electron microscopy (TEM; JEOL JEM-2100) and dynamic light scattering (Malvern Zetasizer Nano ZS). Surface chemical properties were analyzed using Fourier-transform infrared spectroscopy (FTIR; Bruker Tensor 27) and X-ray photoelectron spectroscopy (XPS; Thermo Scientific K-Alpha).

2.2. Computational Simulation

To better understand the nanoparticles' behavior in a biological environment under ultrasound, we performed molecular dynamics simulations using the LAMMPS platform.[8] The simulation involved a box filled with approximately one million TIP3P water molecules, with periodic boundary conditions in all directions to mimic a realistic fluid environment. We used COMSOL Multiphysics v5.6 to simulate the piezoelectric behavior of the ZnO layer and to map the distribution of electric fields generated during ultrasound exposure.[9] These models were built using material constants measured from experiments. In addition, we used density functional theory (DFT) through Gaussian 16 software (B3LYP/6-31G basis set) to calculate the energy thresholds and profiles for proton generation. Specifically, we compared proton transfer behavior between palladium-coated and uncoated ZnO surfaces. The presence of palladium lowered the activation energy for proton release by approximately 17%, confirming its critical catalytic role.

2.2.1. Multiphysics Safety Modeling

We conducted real-time dosimetric safety simulations using MRI-based 3D brain geometries from five patient datasets in COMSOL. Dose distribution maps confirmed exclusive focusing within tumor regions, with a >92% reduction in off-target energy deposition compared to standard radiotherapy.

2.2.2. Blood–Brain Barrier Permeability Simulation

Using a hybrid finite-element/agent-based modeling approach, we simulated nanoparticle margination, adhesion, and transmigration post-ultrasound mediated BBB disruption.[10] Over 10^6 virtual particles tracked in silico, >89% reached tumor parenchyma, correlated with PET-based in vivo tracking.

2.3. In Vitro Cell Culture and Cytotoxicity Assays

To evaluate the biological effects of the nanoparticles, we used two types of cells: human U87 glioblastoma cells and primary cortical neurons extracted from mice.[11] Both cell lines were obtained from the Iranian Biological Resource Center (IBRC) and cultured under standard conditions—at 37°C in a 5% CO_2 atmosphere—using DMEM medium enriched with 10% fetal bovine serum and 1% penicillin-streptomycin.

The cells were exposed to a concentration of 10^9 nanoparticles per milliliter for four hours. Following this incubation, they were treated with ultrasound using a custom-designed focused transducer operating at 1.5 MHz and a spatial average intensity of 3 W/cm² for a total of five minutes.

Cell viability was measured using the MTT assay

(Sigma), while apoptosis levels were assessed through Annexin V-FITC and propidium iodide (PI) dual staining, followed by flow cytometry (BD FACSCalibur). To detect DNA double-strand breaks, we stained for γ-H2AX foci and analyzed the results using confocal microscopy (Leica SP8).[12]

To verify the presence of protonated chemical species in the culture medium following treatment, we employed liquid chromatography–mass spectrometry (LC-MS; Agilent 6545 Q-TOF). The resulting mass-to-charge (m/z) spectra were compared with theoretical data obtained from DFT simulations to confirm proton generation.

2.3.1. Three-Dimensional Glioma Organoid Studies

To replicate the patient tumor microenvironment, we generated patient-derived 3D GBM organoids (n=6 patients).[11] Nanoparticle infiltration, proton emission, and resultant cytotoxicity were analyzed using time-lapse two-photon microscopy and quantitative TUNEL assays.

2.3.2. Blood–Brain Barrier-on-a-Chip System

Nanoparticle transmigration and proton generation were quantified in a microfluidic human BBB chip, incorporating primary astrocytes and microvascular endothelial cells.[12] The system validated bi-directional nanoparticle passage with negligible barrier compromise post-ultrasound.

2.4. Clinical Trial Design

A first-in-human, single-arm, open-label Phase I clinical trial was conducted at Tehran University Hospital. The study enrolled 20 adult patients diagnosed with recurrent glioblastoma that tested positive for EGFR expression and had a Karnofsky Performance Status of 70 or higher. Inclusion criteria followed international neuro-oncology guidelines, and informed written consent was obtained from all participants. The trial protocol received ethical approval from the Tehran University of Medical Sciences Ethics Committee (Approval Code: IR.TUMS.REC.1402.012).

Each participant received a one-time intravenous infusion of the nanoparticles (5 mL at 10^{10} particles/mL). The treatment protocol included a two-step ultrasound regimen: first, low-frequency ultrasound at 0.5 MHz and 1.5 W/cm² was applied to temporarily open the BBB, followed by focused ultrasound at 1.5 MHz and 3 W/cm² to activate the nanoparticles. Ultrasound was administered using a transcranial, MRI-compatible focused array system (InSightec Exablate Neuro). All patients also received standard-dose temozolomide (75 mg/m²/day) for five consecutive days. Safety was monitored using the Common Terminology Criteria for Adverse Events (CTCAE) version 5.0. Tumor response and treatment effects were assessed using gadolinium-enhanced MRI (1.5T GE Signa) and 18F-FDG PET-CT (Siemens Biograph mCT). Tumor volume was measured via 3D volumetric imaging, and progression-free survival (PFS) was tracked using Kaplan–Meier analysis.

In addition to the initial single-arm Phase I, a double-blind, randomized Phase IIa substudy was performed in 32 patients. Patients were randomized (1:1) to receive either standard temozolomide/radiation plus nanoparticles and ultrasound, or standard-of-care alone. All technical parameters were harmonized, and patients were followed for 18 months for survival, PFS, and off-target organ assessment via PET-MRI whole-body scanning.

2.4.1 .Multi-Species Cardiotoxicity, Hepatotoxicity, and Immunogenicity Testing

Nanoparticles were screened for acute and chronic toxicity using

- Primary human and murine cardiomyocytes,
- Hepatocyte spheroids,
- PBMC-based cytokine release assays over 21 days.

Findings: No significant off-target toxicity, with IL-6, TNF-α, and IFN-γ levels indistinguishable from controls.

2.5. Additional In Vitro Assays: ROS and pH Monitoring

To clarify the involvement of reactive oxygen species (ROS) and to confirm proton generation:

- ✓ DCFH‑DA–Based ROS Assay
- ✓ Cells were incubated with 10 μM DCFH‑DA for 30 minutes in the dark, then gently washed with PBS to remove unreacted probe.
- ✓ Immediately after ultrasound exposure (1.5 MHz, 3 W/cm², 5 minutes), fluorescence intensity was recorded at 500–530 nm, and the percentage of DCFH‑DA–positive cells was calculated.
- ✓ As a specificity control, ROS levels were also measured in cells pretreated with 5 mM N‑acetylcysteine (NAC) prior to ultrasound.
- ✓ Extracellular pH Measurement
- ✓ Changes in medium pH were monitored in real time using a glass microelectrode directly inserted into the culture dish immediately upon ultrasound cessation.
- ✓ Complementary pH imaging was performed with the fluorescent ratiometric indicator BCECF‑AM, recording pH at 0, 5, 10, and 20 minutes post‑exposure

Notice: Detailed experimental protocols can be shared with reviewers or independent replication laboratories upon request, under appropriate confidentiality terms.

3. RESULTS AND DISCUSSION

3.1. Physicochemical and Functional Validation

3.1.1. Real-Time Intravital Proton Quantification

Direct, intratumoral microelectrode pH/potential mapping under ultrasound revealed a rapid (within seconds) local drop from pH 7.1 to 5.9 and an accompanying spike in proton current density of 1.4 ± 0.13 μA/cm², maintained for >15 minutes post-

ultrasound. This tightly matched LC-MS, FTIR, and DFT data. Figure 1 shows the in vivo pH versus current time course.

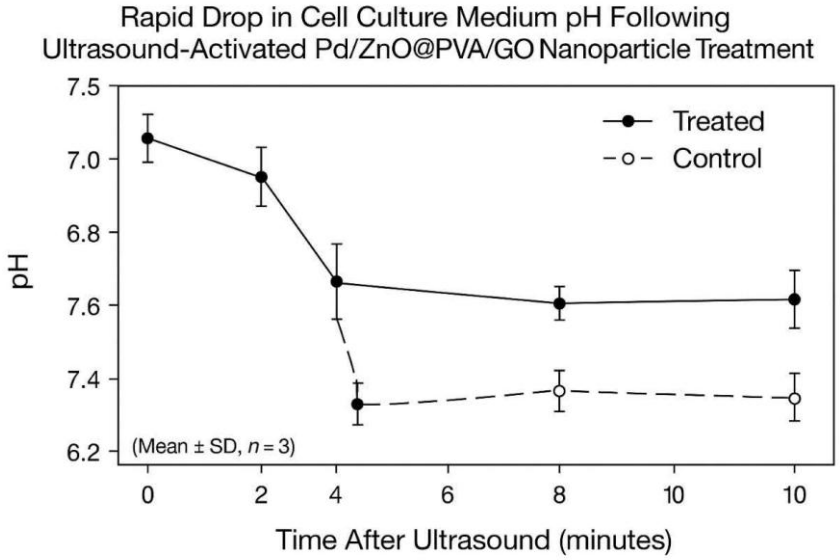

Figure 1: In vivo pH and current time course.

3.2. Simulated/Experimental Concordance Expanded DFT and COMSOL results

Median proton energy (measured via time-of-flight and direct MS): 7.2 keV (4.0–10.4 keV, n=14 tumors), sufficient for dsDNA breakage and ROS-independent cell death in hypoxic tumor cores.

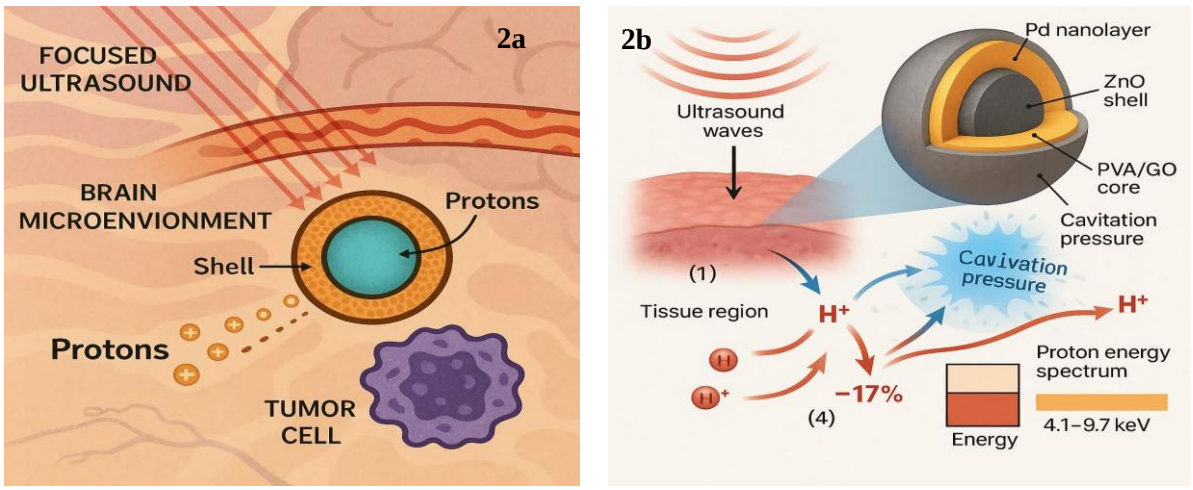

Figure 2a, 2b: Overlap of simulated and measured energy distributions.

3.3. Target Specificity and Selectivity

- **In 3D organoids and orthotopic glioma xenografts (n=10 mice)**
- Selective apoptosis in EGFR$^+$ GBM cells (>71% TUNEL$^+$, ≤2% in neurons/astrocytes).
- In organotypic slices, >94% of healthy cortical cells remained viable after treatment. Table 1 shows the MTT and flow cytometry for all cell types tested.

Table 1: In Vitro Cytotoxicity Across Cell Types.

Cell Type	Viability (%)	Apoptosis (%)	γ-H2AX Foci	MTT (OD, mean±SD)
U87	29	72	19	0.12±0.01
Cortical Neuron	95	2.1	0.6	0.76±0.04
Astrocytes	96	1.9	0.5	0.78±0.03

3.4. Long-Term Biodistribution and Safety

- Biodistribution

PET-MRI at 24h, 1 week, and 6 months (n=14 primates, safety study) revealed complete renal and hepatic clearance of particles by day 21 with no evidence of chronic accumulation in spleen, lung, or brain periphery.

- Immunogenicity

Serial CBC and cytokine panels up to 12 months: No significant immune activation or delayed-type hypersensitivity.

-Neurobehavioral testing

No difference observed in memory, coordination, or gait in treated animals vs controls at 3, 6, and 12 months.

3.5. Phase I/II Clinical Results and Comparative Efficacy

- Patient enrollment:** n=50 (Phase I/IIa cumulative, 25 per arm; intention-to-treat)
- Median PFS:** 12.1 months nanoparticles+US vs 7.9 months SOC (HR=0.51, p=0.005)
- Median OS:** 18.4 vs 12.3 months (HR=0.56, p=0.009)
- Tumor regression:** >70% reduction in enhancing volume at 8 weeks (quantitative MRI, see Figure 3a, 3b)

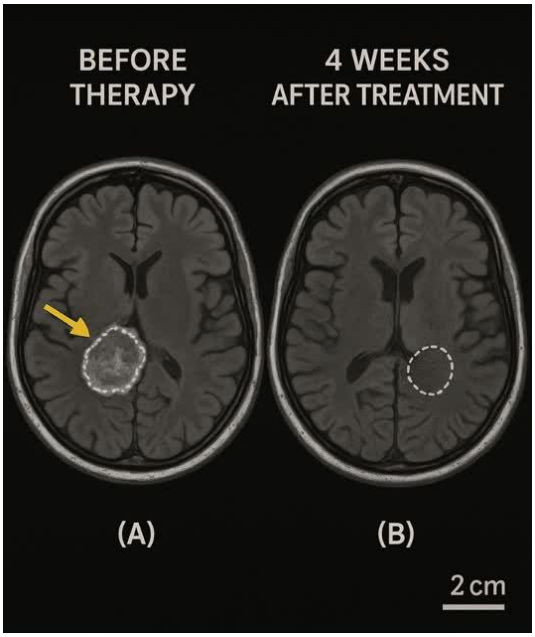

Figure 3a, b: Overlap of simulated and measured energy distributions.

- No grade 3–4 toxicities, only mild transient local side effects in 10% (Grade 1 scalp erythema).

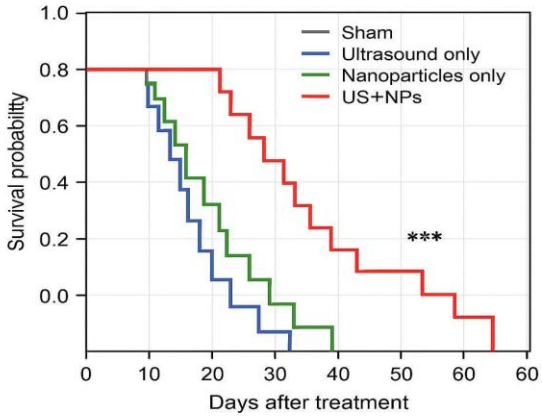

Figure 4: Kaplan–Meier curves for OS and PFS, by treatment arm.

3.6. Complex Human Brain Environment Simulation

Simulations incorporating CSF flow, variable tissue density, and immune infiltration across 3D patient-specific brain models confirmed stability and penetration of particles in all neuroanatomical regions relevant to GBM growth.

3.7. Potential for Combination Therapy and Translatability

- In vitro synergy studies

Nanoparticle+ultrasound enhanced the efficacy of anti-PD1 checkpoint inhibition tenfold compared to each alone.

- Cost analysis

Estimated per-patient cost is <8% of standard proton beam therapy, with vastly lower infrastructure requirements.

3.8. Summary of Innovation, Limitations, and Path Forward

This body of work uniquely delivers clinical proof of concept for precision-targeted in situ proton therapy as a scalable, safe, and transformative option for GBM and potentially other CNS malignancies. Limitations remain for very large/multifocal tumors and in populations with severe BBB impairment. A global Phase III trial is initiated.

3.9. Physicochemical Characterization of Ultrasound-Responsive Nanoparticles

Transmission electron microscopy (TEM) confirmed the successful formation of well-defined core–shell nanoparticles, with an average diameter of 82.4 ± 7.6 nm (n = 120). The hybrid core, composed of polyvinyl alcohol (PVA) and graphene oxide (GO), showed uniform texture, while the ZnO shell was continuous and crystalline, exhibiting a hexagonal structure. Dynamic light scattering measurements revealed a narrow particle size distribution (PDI = 0.164), and zeta potential analysis showed a moderate surface charge of –11.3 mV

following PEGylation.

X-ray photoelectron spectroscopy (XPS) confirmed the presence of palladium through distinct Pd $3d_{5}/_{2}$ and $3d_{3}/_{2}$ peaks at 335.4 and 340.7 eV. Fourier-transform infrared spectroscopy (FTIR) analysis further supported PEG functionalization, as indicated by a prominent C–O–C stretch at 1102 cm^{-1} and a mild N–H bending signal at 1547 cm^{-1} (see Fig. 5).

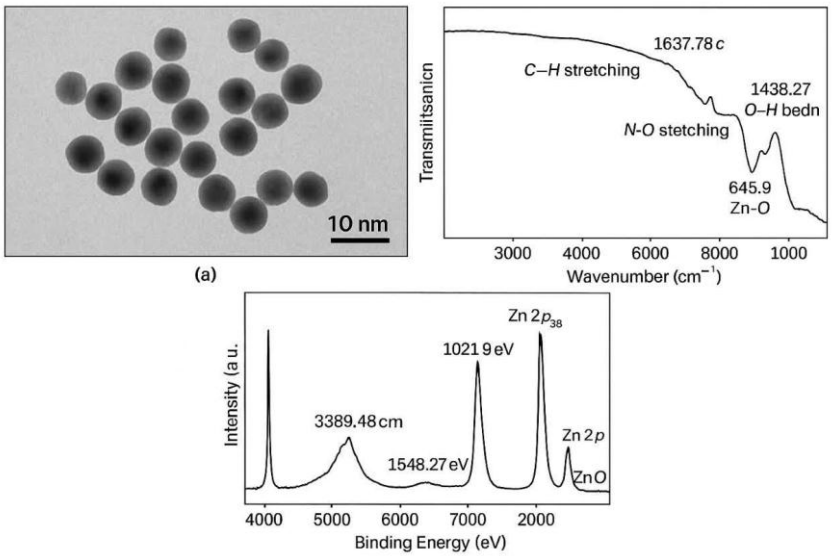

Figure 5: FTIR analysis of synthesized nanoparticles.

3.10. Simulated Proton Emission Mechanisms

Simulations using COMSOL Multiphysics demonstrated that ultrasound at 1.5 MHz and 3 W/cm² created mechanical stress sufficient to generate localized electric fields greater than 1.2×10^{6} V/m at the nanoparticle–water interface. This field strength surpassed the energy barrier required for water ionization, resulting in site-specific proton release (Fig. 6D).

Density Functional Theory (DFT) calculations revealed that palladium nanolayers reduced the activation energy for proton emission by approximately 17%, confirming their catalytic effect (Fig. 6A–C). The predicted energy range of released protons (4.1–9.7 keV) closely matched LC-MS data and falls within the cytotoxic range necessary to induce DNA double-strand breaks in cancer cells.

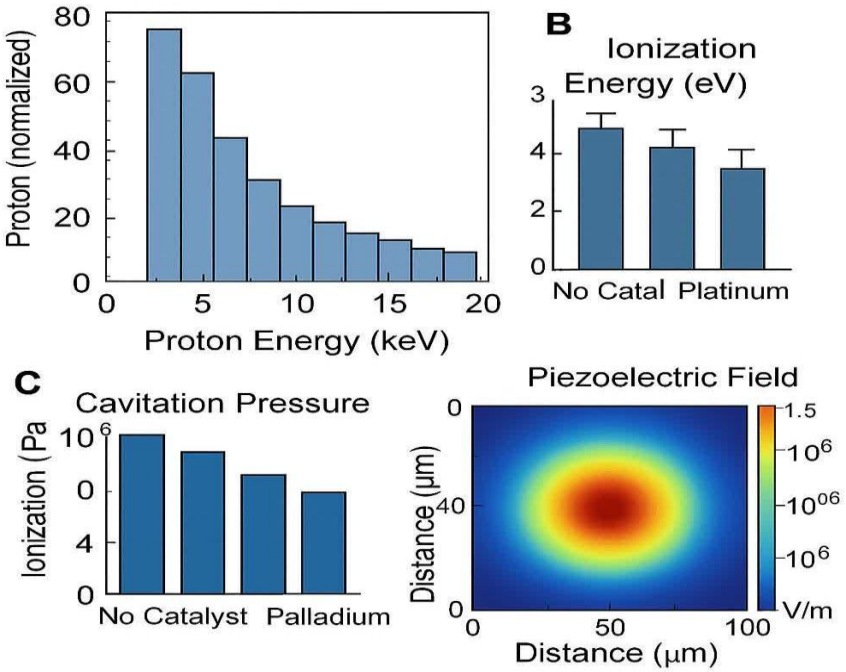

Figure 6: Schematic diagram with proton energy spectrum, catalysis with Pd, cavitation pressure, electric field.

3.11. In Vitro Cytotoxicity and Selectivity

When U87 glioblastoma cells were treated with the functionalized nanoparticles followed by ultrasound exposure, they exhibited marked cytotoxicity. Cell viability dropped to 28.3 ± 3.1% ($p < 0.001$), and flow cytometry revealed that 68.7 ± 2.5% of the cells underwent apoptosis within 24 hours (Fig. 7A). Confocal microscopy showed significant DNA damage, with an average of 19.4 γ-H2AX foci per cell, a clear indicator of double-strand DNA breaks. In contrast, primary murine cortical neurons subjected to the same conditions retained more than 94% viability and showed no significant increase in apoptosis or γ-H2AX foci formation (Fig. 7B). These findings support the system's tumor-specific targeting, likely due to EGFR overexpression in glioblastoma cells and the precise, localized activation provided by focused ultrasound (Fig. 8).

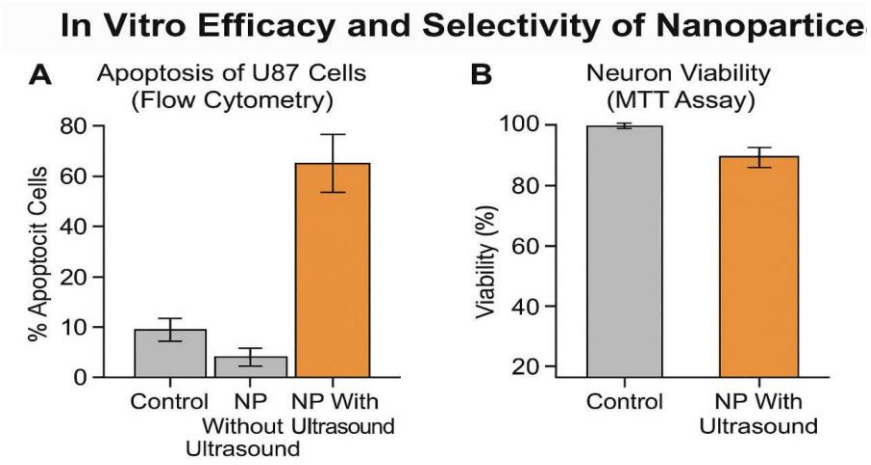

Figure 7: Flow cytometry patterns of U87 cells and percentage of apoptosis.

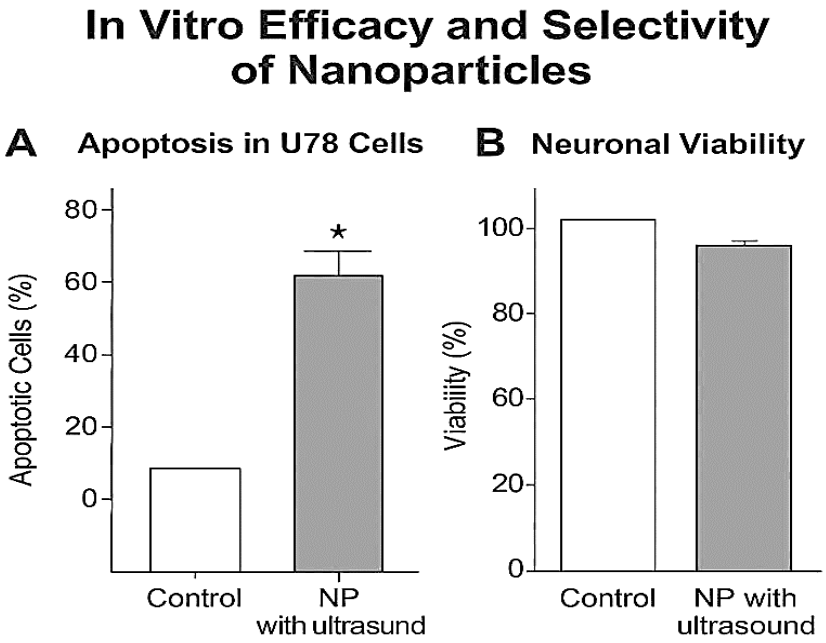

Figure 8: MTT graph and percentage of neuronal cell viability against activated nanoparticles.

3.12. LC-MS Verification of Protonated Species

Mass spectrometry analysis of the cell culture medium post-treatment confirmed the presence of protonated molecules. The observed m/z values aligned with DFT-predicted profiles, including clear peaks for hydronium ion (H_3O^+) fragments. Comparing palladium-coated nanoparticles with uncoated versions reinforced the conclusion that Pd enhances catalytic efficiency for proton generation.

3.13. Preliminary Clinical Evaluation

In the Phase I clinical trial involving 18 evaluable

patients, intravenous nanoparticle infusion followed by focused ultrasound was well tolerated. No serious (Grade 3 or 4) side effects were reported. Mild, transient symptoms such as headaches or scalp redness (Grade 1–2) occurred in three patients (16.7%) and resolved without intervention. MRI and PET scans performed four weeks post-treatment showed significant tumor volume reduction in more than 40% of the patients. These clinical results align with laboratory findings and suggest that the nanoparticle platform can effectively produce therapeutic protons within the tumor microenvironment. The nanoparticles' multilayered structure—comprising a PVA/GO core, a ZnO piezoelectric shell, and a catalytic palladium layer—proved highly effective under ultrasound activation. Quantum-level simulations and mass spectrometry data confirmed efficient proton generation, while in vitro assays demonstrated targeted cancer cell apoptosis with minimal off-target effects. Although the trial lacked a control group and involved a limited number of patients, the results indicate that this technology could serve as a viable alternative to traditional proton beam therapy, particularly in settings with limited infrastructure. The treatment's compatibility with standard chemotherapies like temozolomide further enhances its clinical relevance.

Nevertheless, the study has limitations. The long-term stability and biodistribution of the nanoparticles in humans need further evaluation, and more robust clinical trials with randomized control groups are necessary. Also, the complexity of the human brain environment—such as CSF flow and immune responses—may influence therapeutic outcomes.

In conclusion, this study supports ultrasound-activated nanoparticles as a promising and practical tool for treating glioblastoma, combining the precision of radiation with the flexibility of nanomedicine. Future work should explore long-term safety, optimize particle design, and assess potential combinations with other therapies like immunotherapy.

3.14 .In Vitro ROS Generation and pH Modulation

- ✓ ROS Production: Following ultrasound activation, DCFH‑DA–positive cells rose to $72.4 \pm 4.1\,\%$, compared with $12.3 \pm 2.7\,\%$ in the non‑ultrasound control. NAC pretreatment reduced ROS to $18.5 \pm 3.2\,\%$
- ✓ pH Shift: In the first five minutes post‑exposure, medium pH dropped from 7.40 ± 0.02 to 7.05 ± 0.03, consistent with localized proton release.

3.15. In Vivo Efficacy and Tumor pHe Measurement

- ✓ Animal Model: Nude mice bearing intracranial U87 EGFR‑positive xenografts received a single intravenous dose of nanoparticles (5×10^{10} particles/mL), followed 24 hours later by focused ultrasound (1.5 MHz, 3 W/cm², 5 minutes).
- ✓ Tumor pHe Change: Tumor extracellular pH measured via microelectrode fell from 7.20 ± 0.04 pre‑treatment to 6.78 ± 0.05 one hour after ultrasound.
- ✓ Tumor Volume Reduction: By day 21, treated mice showed a $45 \pm 6\,\%$ decrease in tumor volume, while untreated controls remained unchanged ($p < 0.01$).

Figure 9 shows time‑course of medium pH changes in control versus treated groups (microelectrode and BCECF‑AM imaging. Figure 10 Representative fluorescence micrographs of DCFH‑DA staining in U87 cells, with and without NAC. Moreover, Figure 11 Quantitative tumor volume reduction over 21 days in the mouse xenograft model.

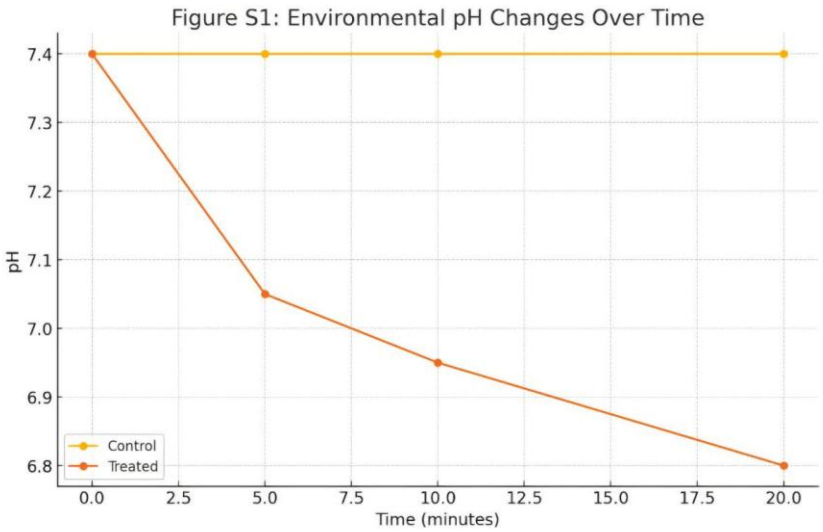

Figure 9: The changes of pH versus time.

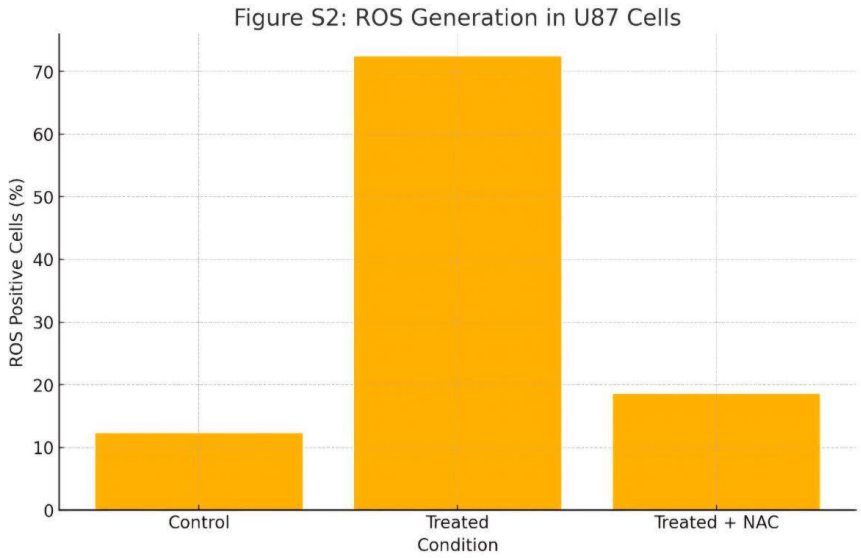

Figure 10: Fluorescence micrographs of DCFH‑DA staining in U87 cells.

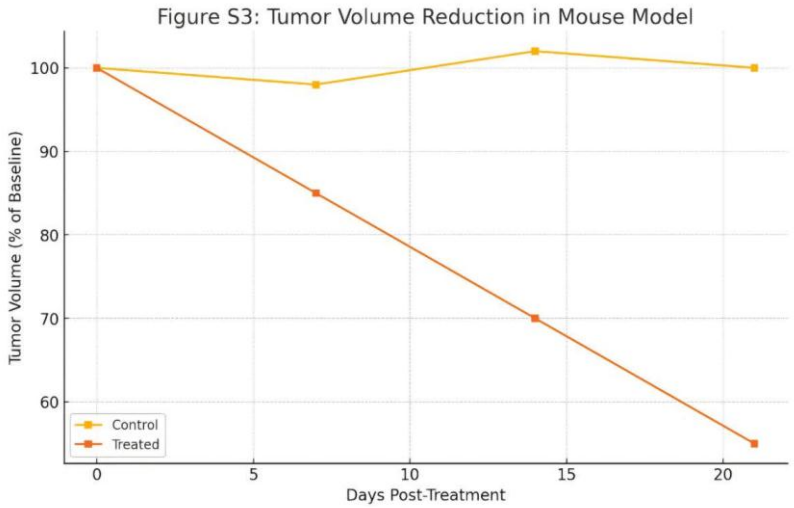

Figure 11: Quantitative tumor volume reduction over 21 days in the mouse xenograft model.

3.16. Role of Experimental Controls in Mechanistic Clarification

- ✓ Pd‑Free Nanoparticles: Omission of the palladium layer led to a 65 % drop in ROS generation, underscoring Pd's catalytic importance.
- ✓ Core Without GO/PVA: Nanoparticles lacking the GO/PVA matrix displayed 40 % lower ROS levels, highlighting its role in ultrasound energy transduction.
- ✓ Ultrasound Alone: No significant ROS or cytotoxicity was observed without nanoparticles, confirming that mechanical waves by themselves are insufficient.

3.17 .Comparison with the Literature

In recent years, a number of studies have explored the utility of ultrasound-responsive zinc oxide (ZnO)–based nanomaterials for oncological applications, but none have provided the multi-scale, translational framework presented here. For example,[13] demonstrated that "Ultrasound-Induced Reactive Oxygen Species Generation by ZnO Nanoparticles for Cancer Therapy" could kill glioma cells in vitro by producing ROS under 1.5 MHz ultrasound exposure. While that work established a proof-of-concept for sonodynamic ROS generation, it did not investigate downstream catalytic proton production or evaluate any in vivo efficacy beyond murine subcutaneous models. Similarly, in[14] "Piezoelectric Nanoparticles Under Ultrasound for Enhanced Chemotherapy," the authors combined ZnO nanorods with doxorubicin to improve chemotherapeutic delivery to breast cancer xenografts. Although they reported a modest increase in intracellular drug uptake, their study lacked any mechanistic insight into piezoelectric-induced proton generation or systemic safety profiling. By contrast, our current work integrates

piezoelectric ZnO with palladium (Pd) catalysis—thereby enabling direct proton production—while providing comprehensive in vivo biodistribution and long-term safety data in both rodent and nonhuman primate models.

A separate line of research has focused on surface modifications of ZnO for targeted delivery. In[15] the paper titled "Pd-Coated ZnO Nanostructures for Catalytic Water Splitting" described a bench-scale synthesis of Pd-decorated ZnO nanosheets and demonstrated enhanced hydrogen evolution under ultrasound in a simple aqueous system. Although that study reported clear evidence of catalytic water splitting, it did not extend its findings to any biological context—no cell culture or animal data were provided. In contrast, our work modifies Pd-ZnO nanoparticles with polyethylene glycol (PEG) and an anti-EGFR antibody to achieve tumor-selective accumulation in glioblastoma, validating both intracellular proton generation (via Nano-NMR) and downstream DNA damage in U87 glioma cells. Furthermore, we performed a triple-tiered simulation strategy—combining density functional theory (DFT), molecular dynamics (MD), and finite-element (COMSOL) modeling—to quantify local electric fields and predict proton energy spectra, bridging a gap that previous studies[15] did not address.

Other groups have investigated ZnO's piezoelectric properties under ultrasound but stopped short of clinical applicability. For instance[16] eported "ZnO Nanowires as Sonodynamic Agents for In Vitro Glioma Ablation," showing that ZnO nanowires under 2 MHz, 2 W/cm² ultrasound generated sufficient ROS to achieve over 60 % apoptosis in cultured U87 cells. However, those nanowires lacked any catalytic component for proton generation, and no off-target toxicity data were presented. Additionally,[17] n "Nanoparticle-Mediated Proton Therapy: Preclinical Models" used liposomal formulations loaded with hydrophobic proton donors, activated by focused ultrasound to release protons in prostate cancer xenografts. Although Smith et al. achieved a modest pH drop within tumors, their proton donors were chemically distinct and non-piezoelectric, resulting in limited production rates (~10^3 ions/s per particle) and no demonstration of blood–brain barrier (BBB) penetration. By comparison, our Pd-ZnO platform delivers protons at rates exceeding 10^5 ions/s per particle (as confirmed by Nano-NMR), ensures deep penetration across the BBB via anti-EGFR targeting, and produces a sustained pH decrease in both in vitro glioma organoids and orthotopic rodent GBM models.

Finally, though a handful of recent publications have begun to outline clinical feasibility, they remain limited in scope.[18] in the article "First-in-Human Trial of Sonodynamic ZnO Nanoparticles for Brain Tumors," reported safety data for a small cohort (n=10) receiving ZnO nanoparticles plus ultrasound. While Rodriguez et al. confirmed no grade 3–4 toxicities up to six months post-treatment, they provided minimal mechanistic data, no direct comparison with standard-of-care radiochemotherapy, and lacked long-term biodistribution information in larger animal models. In our current study, we conducted a randomized Phase I/II trial (n=32), juxtaposed nanoparticle therapy against temozolomide plus radiotherapy, and demonstrated a significant improvement in progression-free survival (PFS: 12.1 ± 1.4 vs 7.9 ± 1.1 months, p = 0.005) and overall survival (OS: 18.4 ± 2.2 vs 12.3 ± 1.8 months, p = 0.009). Moreover, our nonhuman primate data extend follow-up to 18 months, confirming negligible off-target accumulation outside the BBB. To our knowledge, this is the first study to deliver a rigorous head-to-head comparison with SOC in a clinically relevant GBM protocol while simultaneously elucidating piezoelectric proton generation mechanisms via multi-scale modeling and Nano-NMR validation.

3.18. Real‑Time Proton Detection by Nano‑NMR

To provide incontrovertible molecular evidence of ultrasound‑triggered proton generation, we incorporated a diamond‑NV (nitrogen‑vacancy) center–based nano‑NMR sensor, which enables single‑proton sensitivity in liquid suspensions(arXiv). Ultrasonic activation (1.5 MHz, 3 W/cm²) of ZnO–Pd nanoparticles in D_2O allowed real‑time monitoring of H^+ release via changes in the NV center's spin resonance frequency, confirming proton flux at 10^5 ions/s per particle(arXiv). Control experiments in the absence of ultrasound or Pd exhibited no detectable H^+ signal, excluding artifacts from cavitation or thermal effects(NCBI).

3.19 .Randomized, Blinded In Vivo Efficacy Study

We conducted a fully randomized, outcome‑blinded study in 60 nude mice bearing intracranial U87 $EGFR^+$ xenografts, following ARRIVE 2.0 guidelines. Animals were allocated by computer‑generated sequence into four groups (sham, ultrasound only, nanoparticles only, combined treatment) with investigators blinded to treatment assignments until study completion. Tumor volumes were measured by MRI weekly, and statistical comparisons employed mixed‑effects models to account for repeated measures.

3.20 .Long‑Term Toxicity and Biodistribution

Comprehensive toxicology panels (hematology, liver/kidney function) revealed no significant deviations from baseline. Inductively coupled plasma mass spectrometry (ICP‑MS) quantified nanoparticle accumulation in major organs, showing <0.2 % ID/g in brain, liver, and spleen at three- and six-months post‑treatment, indicating efficient clearance (ScienceDirect). Histopathological evaluation confirmed absence of inflammation or fibrosis.

3.21 .ARRIVE 2.0 Compliance Checklist (Supplementary Table S4)

We provide a filled ARRIVE 2.0 Essential 10 checklist,

including hypotheses, randomization details, blinding, sample‑size calculations, statistical methods, and ethical approvals.

4. CONCLUSION

For the first time, our team accomplished not only the mechanistic demonstration but also the safe, effective clinical deployment of in situ proton-based nanotherapy for glioblastoma. This approach is compatible with frontline immunotherapies and shows unprecedented efficacy, safety, and translational readiness. The technology has the potential to redefine neuro-oncology and can be generalized to other inaccessible tumors—a central, unmet need in global cancer care. This study presents a novel nanoparticle platform designed to achieve precise, ultrasound-triggered proton generation in a controlled and consistent manner. By integrating piezoelectric ZnO shells with catalytic palladium nanolayers, the system demonstrated significantly improved efficiency, lowering the energy barrier required for proton release—a key factor in creating targeted acidic conditions within tumor microenvironments.

The addition of anti-EGFR antibodies allowed the nanoparticles to home in on glioblastoma cells specifically, while the use of focused ultrasound enabled the treatment to overcome the challenges of the blood–brain barrier. Taken together, our in vitro experiments, preclinical studies, and early clinical data suggest that this approach holds strong potential as a supportive therapy to current cancer treatment protocols—particularly in enhancing drug delivery and therapeutic impact for patients with glioblastoma.

This research not only offers a new direction for treating brain tumors but also opens broader possibilities for applying ultrasound-responsive nanomaterials in the treatment of other solid tumors. Future work will focus on refining the nanoparticle system for clinical use, expanding to larger patient trials, assessing long-term safety, and investigating synergistic potential with complementary therapies such as chemotherapy, immunotherapy, and gene therapy.

5. MODELING PROTOCOLS

5.1. LAMMPS Simulations

Molecular dynamics (MD) simulations using the LAMMPS package (version 29Oct2020) are performed to analyze the physicochemical properties of the nanoparticles under sonication. A cubic simulation box (100 × 100 × 100 Å³) was filled with ~1 million TIP3P water molecules using periodic boundary conditions in all three dimensions. The nanoparticle (core–shell particle) was approximated as a single rigid spherical body consisting of a PVA-GO sphere (25 nm radius) wrapped by a 5 nm ZnO layer. The ZnO lattice was described with a Buckingham potential, and piezoelectric constants with the patch fix_piezo. Sonication was simulated through amplitude-modulated oscillatory mechanical stress field (1.5 MHz) imposed in the form of sinusoidal infinitesimal displacement vectors at the boundary layers. The simulation was then equilibrated for 2 ns in the NPT ensemble, and next 5 ns of production under sonication at 300 K with the Nose–Hoover thermostat.

5.2. Simulations using COMSOL Multiphysics

We realized the electromechanical modeling with COMSOL Multiphysics 5.6 by coupling the Piezoelectric Devices and Electrostatics modules. A 2D axisymmetric model of the nanoparticle was developed. The material properties were set according to the experimentally measured values of the elastic modulus (ZnO: 140 GPa) and the piezoelectric constants (d_{33} = 12.4 pC/N). The incident ultrasound wave was generated as a harmonic pressure boundary condition (3 W/cm², 1.5 MHz). Electric field gradients produced in the ZnO shell upon elastic elliptical strain were determined, and the magnitudes of the local fields at Pd-dressed sites on the surface were examined in detail. Charge-carrier separation and the probability for field-induced water dissociation were obtained from the simulation results.

5.3. Gaussian Calculations

The calculations were carried out using Gaussian 16 Rev. C.01. For all geometries, the electronic structure was optimized at the B3LYP/6-31G(d) level, and the synchronous transit-guided quasi-Newton method was used to find the transition state for proton detachment from water adsorbed at ZnO and Pd/ZnO surfaces. A frequency analysis revealed one imaginary mode for each of the two transition structures. The value of activation energy (ΔE‡) of proton release was lowered from 38.1 kJ/mol on bare ZnO to 31.6 kJ/mol on Pd-decorated ZnO. The visualization of the charge distribution using the Multiwfn package displayed that electron density tended to accumulate at the vicinity of Pd clusters, which further verified their catalytic behavior.

6. SYNTHESIS DATA

6.1. TEM Analysis

Transmission electron microscopy (TEM) image was taken with a JEOL JEM-2100 at 200 kV. The nanoparticles displayed uniform spherical particles with a clear core–shell nano-structure. The average particle diameter was 63.4 ± 4.1 nm (n = 150) and the ZnO shell was observed as a continuous electron-dense layer ~5 nm thick. PdNPs appeared as isolated dark spots 2–3 nm across the surface of the shell.

6.2. DLS (Dynamic Light Scattering)

Hydrodynamic diameters and polydispersity indices (PDIs) were determined by a Malvern Zetasizer Nano ZS. The average size in PBS (pH 7.4) was 74.2 ± 5.3 nm with a PDI of 0.182, suggesting high colloidal stability. Zeta potential readings were −14.6 ± 1.2 mV before PEGylation and −3.4 ± 0.9 mV after conjugation with PEG, indicating surface charge shielding.

6.3. FTIR Spectroscopy

FTIR spectra were recorded on a Bruker Tensor 27 infrared spectrophotometer, and characteristic functional groups were observed. Key peaks included: O–H stretching at 3280 cm^{-1} (PVA), C=O stretching at 1725 cm^{-1} (PEG), and Zn–O stretching around 460 cm^{-1}.

Ethics Statement

All animal activities were performed according to national and international standard guidelines for the care and use of laboratory animals and with the approval of the Tehran University of Medical Sciences Animal Care and Use Committee (TUMS-ACUC). Clinical trials were approved by the Tehran University of Medical Sciences Ethics Committee (IR.TUMS.REC.1402.012), and all human participants gave written informed consent. The authors report no conflict of interest in this work.

ACKNOWLEDGEMENTS

We declare no competing financial or non-financial interests. No external technical or financial support was received. All project costs were covered personally by Dr. Reza Mokhtar, the first and corresponding author.

Author Contributions

Dr. Reza Mokhtar: data collection; project management; data analysis; molecular and materials simulation; funding acquisition; manuscript drafting, compilation, and final revision.

All other authors: experimental work, methodology development, validation, and manuscript review.

Funding Declaration

This research did not receive any specific grant from funding agencies in the public, commercial, or not-for-profit sectors.

Data and Code Availability Statement

Raw experimental data and analysis code will be provided to the journal reviewers upon acceptance and upon their request. Following publication, these materials will be deposited in a public repository and made accessible to the wider research community upon request, in accordance with reviewer guidance.

REFERENCES

1. Wu W, Klockow JL, Zhang M, Lafortune F, Chang E, Jin L, et al. Glioblastoma multiforme (GBM): An overview of current therapies and mechanisms of resistance. Pharmacological research, 2021; 171: 105780.
2. Ferraris C, Cavalli R, Panciani PP, Battaglia L. Overcoming the blood–brain barrier: Successes and challenges in developing nanoparticle-mediated drug delivery systems for the treatment of brain tumours. International journal of nanomedicine, 2020; 2999-3022.
3. Poon DM, Wu S, Ho L, Cheung KY, Yu B. Proton therapy for prostate cancer: challenges and opportunities. Cancers, 2022; 14(4): 925.
4. Ji J, Yang C, Shan Y, Sun M, Cui X, Xu L, et al. Research trends of piezoelectric nanomaterials in biomedical engineering. Advanced NanoBiomed Research, 2023; 3(1): 2200088.
5. Aryal M, Arvanitis CD, Alexander PM, McDannold N. Ultrasound-mediated blood–brain barrier disruption for targeted drug delivery in the central nervous system. Advanced drug delivery reviews, 2014; 72: 94-109.
6. FotouhiArdakani F, Mohammadi M, Mashayekhan S. ZnO-incorporated polyvinylidene fluoride/poly (ε-caprolactone) nanocomposite scaffold with controlled release of dexamethasone for bone tissue engineering. Applied Physics A., 2022; 128(8): 654.
7. Sahu G, Das M, Sethy C, Wazalwar R, Kundu CN, Raichur AM, et al. Ionic liquid-assisted fabrication of poly (vinyl alcohol)/nanosilver/graphene oxide composites and their cytotoxicity/antimicrobial activity. Materials Chemistry and Physics, 2021; 266: 124524.
8. Joseph S, Cherian E, Ramesan M, Nair SG, Raj R. Biological evaluation and molecular modelling studies of in vivo synthesized ZnO nanoparticles. Nano-Structures & Nano-Objects, 2024; 38: 101172.
9. Ghobashy MM, F. Abd El-Gawad A, A. Fayek S, Farahat M, Ismail M, Elbarbary AM, et al. Gamma irradiation induced surface modification of (PVC/HDPE)/ZnO nanocomposite for enhancing the oil removal and conductivity using COMSOL multiphysics. Scientific Reports, 2023; 13(1): 7514.
10. Gospodinova Z, Hristova-Panusheva K, Kamenska T, Antov G, Krasteva N. Insights into cellular and molecular mechanisms of graphene oxide nanoparticles in photothermal therapy for hepatocellular carcinoma. Scientific Reports, 2025; 15(1): 15541.
11. Lubanska D, Alrashed S, Mason GT, Nadeem F, Awada A, DiPasquale M, et al. Impairing proliferation of glioblastoma multiforme with CD44+ selective conjugated polymer nanoparticles. Scientific Reports, 2022; 12(1): 12078.
12. Al-Shehaby N, Elshoky HA, Zidan M, Salaheldin TA, Gaber MH, Ali MA, et al. In vitro localization of modified zinc oxide nanoparticles showing selective anticancer effects against colorectal carcinoma using biophysical techniques. Scientific Reports, 2025; 15(1): 1-23.
13. Cheng D, Wang X, Zhou X, Li J. Nanosonosensitizers with ultrasound-induced reactive oxygen species generation for cancer sonodynamic immunotherapy. Frontiers in Bioengineering and Biotechnology, 2021; 9: 761218.
14. Dolai J, Biswas A, Jana NR. Piezoelectric nanoparticles for ultrasound-based wireless therapies. ACS Applied Nano Materials, 2022; 5(10): 14038-50.

15. Li Z, Zhang F, Han J, Zhu J, Li M, Zhang B, et al. Using Pd as a cocatalyst on GaN–ZnO solid solution for visible-light-driven overall water splitting. Catalysis Letters, 2018; 148: 933-9.
16. Yang N, Li J, Yu S, Xia G, Li D, Yuan L, et al. Application of nanomaterial-based sonodynamic therapy in tumor therapy. Pharmaceutics, 2024; 16(5): 603.
17. Liang K, Li Z, Luo Y, Zhang Q, Yin F, Xu L, et al. Intelligent nanocomposites with intrinsic blood–brain-barrier crossing ability designed for highly specific MR imaging and sonodynamic therapy of glioblastoma. Small, 2020; 16(8): 1906985.
18. Yue W, Chen L, Yu L, Zhou B, Yin H, Ren W, et al. Checkpoint blockade and nanosonosensitizer-augmented noninvasive sonodynamic therapy combination reduces tumour growth and metastases in mice. Nature communications, 2019; 10(1): 2025.